Front Range Community College - Larimer Campus

PRISM DemoSat Team

Photonics Research Involving Space Mechanics

Solar Irradiance and Atmospheric Composition: Correlating Light Levels with Altitude

Mariel Calloway, Lee Nicoletti-Jones, Stephanie Puckett,

Laisha Garcia, Cody Spencer, John McGraw

Advisor: Anne Wrobetz

April 2025

Abstract

Earth's atmosphere is composed of distinct layers that uniquely affect incoming electromagnetic radiation in the form of light waves. Substances such as oxygen, ozone, water vapor, and particulate matter block or reflect these waves, preventing them from reaching Earth's surface. However, atmospheric windows provide an exception to these effects. These windows are regions in the atmosphere where light waves are not fully absorbed, allowing electromagnetic radiation of specific wavelengths, particularly visible and infrared light, to pass through. Since light filtration depends on the atmospheric composition at a given altitude, one of the key questions our project aimed to answer was: *How do light levels vary with altitude?*

Equipped with a spectrometer, a pressure sensor, and an air quality sensor, our team collected data during the ascent and descent of a DemoSat weather balloon payload to examine how light intensity correlates with altitude changes and air composition. We also measured particulate matter, anticipating that wildfire pollution could influence light transmission. This data was compared with historical estimates to observe seasonal changes.

Our findings showed that all light intensity readings increased over time in relation to changes in daytime brightness. Certain wavelengths experienced dips that correlated with peak altitude, while some wavelengths experienced their maximum values at lower altitudes only. We examined our data by correlating altitude and solar irradiance to determine trends. This paper outlines the scientific context, methodology, design overview, and testing process of our payload, along with our findings and their implications for understanding atmospheric effects on light.

Acknowledgements

The PRISM DemoSat team would like to acknowledge and thank Anne Wrobetz, Joe Collins, Ryan Jones, Front Range Community College, EOSS, and the Colorado Space Grant Consortium organizers for providing materials, equipment, guidance, and support with the development and execution of this experiment.

Contents

Section 1

Overview and Underlying Science

1.1 Overview

Atmospheric conditions such as light levels and particulate matter (PM) concentrations vary significantly with altitude changes. As altitude increases above the Earth's surface, atmospheric composition shifts in ways that affect both light filtration and the presence of particulate matter pollution. Studies show incoming light becomes more intense, while pollution tends to decrease (Wild, 2009). These variables can have impacts in several areas, including air quality, solar energy efficiency, human health, and climate pattern modeling.

1.2 Light Levels and Altitude

The Earth's atmosphere is the lens through which incoming solar light is filtered, and its properties dramatically influence how that light is observed on the surface.

1.2.1 Relationship Between Altitude and Light Intensity

As altitude increases, light levels typically become more intense due to a reduction in atmospheric density and scattering. The key factors driving this increase include:

Decreased Air Molecules: At higher altitudes, the atmosphere contains fewer gas molecules. This results in less light being scattered resulting in less ambient light but increased apparent brightness of the sun. ("Rayleigh Scattering")

Less Absorption and Diffusion: With lower air density, less light is absorbed or diffused, resulting in higher ultraviolet (UV) radiation, decreased blue-shift, and higher apparent magnitude from the sun.

Clearer Skies: Particulate concentrations and water vapor content are lower at higher altitudes, leading to clearer skies and less obstruction of sunlight (Turgut, 2016).

1.2.2 Effects on Solar Radiation

Additional effects on solar radiation that are observed with an increase in altitude include:

Solar Irradiance Levels: Solar Irradiance is the measure of solar energy received per square meter, expressed in watts per square meter. It indicates how much "sunlight power" reaches a surface, directly influencing how much energy solar panels can generate.

Irradiance increases at higher altitudes due to thinner air, which blocks less sunlight compared to lower elevations where more light is scattered or absorbed.

Understanding irradiance is essential for optimizing solar energy use, studying climate, and assessing environmental impacts, especially from UV radiation. It also helps scientists improve solar technologies and predict weather patterns (Serway, 2013).

Increased UV Radiation: UV radiation levels rise with altitude due to reduced atmospheric filtering. For every 1,000 meters (3,280 feet) of altitude gain, UV levels increase by approximately 10-12 percent (Schmucki, 2002).

Brightness and Glare: In high-altitude areas, such as mountainous regions, sunlight appears more intense, which can cause increased glare and eye strain.

1.3 Particulate Matter and Altitude

Particulate matter (PM) refers to tiny particles or droplets in the air. The most common source of PM pollution is due to combustion, either of diesel, gasoline, or from forest fires. While weather patterns can trap and carry particulates to higher elevations, the vast majority of particulate matter is found in the lower troposphere (0-2 km) and concentrations rapidly decrease at higher altitudes (EPA, 2025).

1.3.1 Variation of PM with Altitude

Decreasing PM Concentration: As altitude increases, PM levels generally decrease. Near the ground, human activities (e.g., transportation, industry, and agriculture) generate significant PM emissions. With altitude, these emissions dissipate, resulting in lower PM concentrations (Roostaei et al., 2024).

Boundary Layer Effects: Most PM accumulates in the lower troposphere (0-2 km) due to human activities. Above the planetary boundary layer, PM levels drop significantly.

Influence of Weather Patterns: Atmospheric circulation and weather systems (e.g., temperature inversions) can temporarily increase PM concentrations at mid-altitudes by trapping pollutants.

1.3.2 Altitude Thresholds and PM Distribution:

Low Altitude (0-2 km): High PM concentrations due to vehicular emissions, industrial activities, and natural sources (e.g., dust, pollen, fire) (Roostaei et al., 2024).

Mid Altitude (2-5 km): PM levels gradually decrease as human influence diminishes.

High Altitude (Above 5 km): PM concentrations are minimal, except in cases of wildfires, volcanic eruptions, or stratospheric aerosol events.

1.4 Factors Influencing Variability

Weather Conditions: Wind, temperature, and humidity affect PM distribution and light scattering (EPA, 2025).

Aerosols and Pollution: In urban regions, PM levels may remain elevated at mid-altitudes due to pollution plumes.

Geographic Location: Coastal areas, mountainous regions, and industrial zones exhibit different light and PM patterns due to local environmental factors (Turgut, 2016).

Time of Day and Season: Light intensity varies with the sun's position, while PM levels fluctuate with temperature inversions and seasonal weather patterns.

Section 2

Payload Design and Function

2.1 Project Development and Methodology

2.1.1 Objective

For the Spring 2025 DemoSat project, our team sought a way to record spectral data and to correlate it with various atmospheric conditions. We chose the SparkFun AS7265x Triad Spectroscopy Sensor, capable of recording data across 18 different wavelengths ranging from 410 nm to 940 nm to study this. This device was considered to be the best option for our mass and budget constraints. The primary trade off would be the sacrifice of ultraviolet light data but the gain of infrared data.

With the understanding that atmospheric windows correlate to gas composition of the atmosphere, we would have ideally chosen a detailed air composition sensor capable of detecting gases such as nitrogen, oxygen, ozone, and CO2. However, the sensor options we found that were capable of recording this information were too expensive; they were not feasible for a project of our scope with a limited budget. Instead, we opted for an air quality sensor that could instead measure particulate matter (PM) data. Given the prevalence of wildfires in the western United States, including our home state of Colorado, an awareness of particulate data in the atmosphere would be a valuable tool for measuring the presence of airborne substances that could affect light readings.

2.1.2 Supplies and Cost

Part Name	Source	Cost
Sparkfun QWIIC RedBoard	Purchased	$21.50
Sparkfun AS7265x Triad Spectroscopy Sensor	Purchased	$69.95
Sparkfun QWIIC MicroPressure Sensor	Purchased	$26.95
Sparkfun TMP117 High Precision Temperature Sensor	Purchased	14.95
Sparkfun QWIIC OpenLog	Purchased	$19.95
Adafruit PMSA0031 STEMMA Air Quality Breakout	Purchased	$44.95
Sparkfun QWIIC cable kit	Purchased	$8.95
Tenergy 9V Batteries 8-pack	Purchased	$47.99
Arduino Pro Micro	From personal inventory	-
Solderable breadboard	From personal inventory	-
1/4" Plexiglass sheet	Purchased	$14.99
Nichrome wire, 20 gauge, 50ft	Purchased	$9.99
5V Relay, 2 pack	Purchased	$7.39
DS18B20 waterproof temperature sensor	Purchased	$9.99
PLA 3D printing filament	From personal inventory	-
EVA foam	From FRCC inventory	-
Extruded foam board	From FRCC inventory	-
Aluminum tape	From FRCC inventory	-
M3 hardware	From personal inventory	-
Miscellaneous wire and solder	From personal inventory	-
Red LED	From personal inventory	-
5kΩ resistor	From personal inventory	-
330Ω resistor	From personal inventory	-
Battery connectors	Homemade	-
Switches	From FRCC inventory	
Various resistors	From personal inventory	-
Flight tube	Given to us by COSGC	-
Total		$297.52

Figure 2.1: Parts and Cost

2.2 Hardware

The primary objective of the payload was to observe changes in light intensity with respect to altitude. To achieve this, we used the SparkFun AS7265x Triad Spectroscopy Sensor, capable of measuring 18 discrete wavelengths across the visible and infrared spectra. As a secondary objective we also aimed to correlate light intensity with particulate concentration by incorporating the Adafruit PMSA0031 Air Quality Sensor, which measures PM1.0, PM2.5, and PM10.0 using laser scattering. To estimate altitude, we included the SparkFun TMP117 High Precision Temperature Sensor and the SparkFun Micropressure Sensor. All sensor data was logged to a microSD card via the SparkFun OpenLog module.

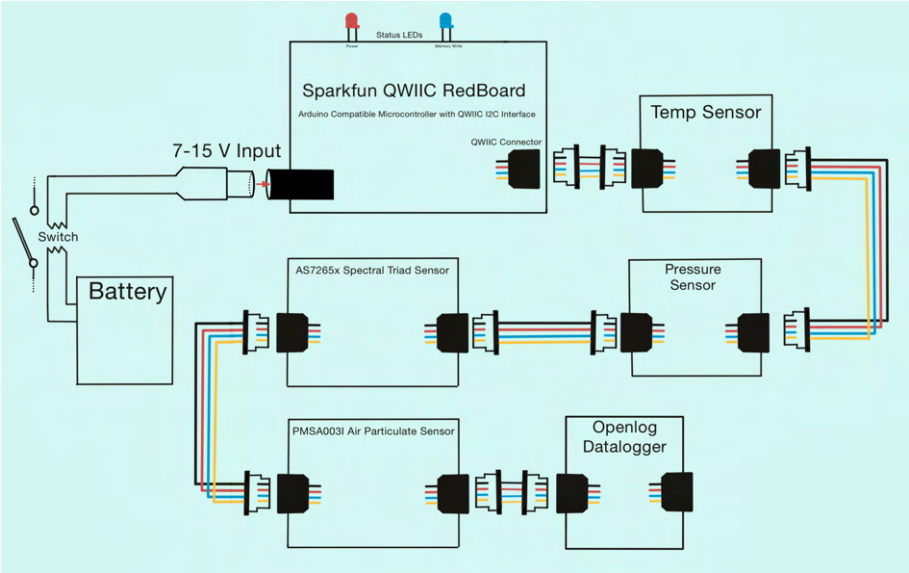

Figure 2.2: Sensor Array Schematic

2.2.1 Heating Subsystem

Based on data from a prior test flight, we determined that active heating would be necessary to ensure continued sensor functionality. After evaluating several options, we decided the cheapest and simplest option would be a custom heating subsystem comprising of an Arduino Pro Micro, DS18B20 temperature sensor, 5V relay, and a nichrome wire coil. The DS18B20 was chosen for its simple operation and long cable length, allowing for strategic placement near sensitive components. Nichrome wire (20-gauge) was selected for its appropriate resistance-to-length ratio, allowing compact coil construction with a suitable resistance for 9V power. The coil was mounted on a prototyping breadboard and controlled via relay. A relay was preferred over a transistor for its ability to physically disconnect the heating element in case of malfunction, reducing fire risk. The heating subsystem was controlled by a separate microcontroller than the sensor array to keep its code isolated and facilitate independent testing, improving system reliability.

2.2.2 Spectrometer

The AS7265x was selected based on cost, size, and Qwiic compatibility, which enabled seamless integration with other sensors via I^2C and simplified wiring through a daisy-chain configuration. Although broader-spectrum sensors were initially considered, they were much larger, heavier, and more expensive. Prior applications of the AS7265x that we found on hobbyist forums, such as ambient light sensing for plant growth optimization and portable spectrometry, demonstrated its viability for our use case. Confusingly, the AS7265x sensor is marketed as able to measure ultraviolet wavelengths despite the fact that the lowest wavelength it detects is 410 nm which is outside of the ultraviolet range.

2.2.3 Particulate Sensor

We also explored incorporating a gas sensor, particularly to measure ozone levels since it is a primary contributor to light reflection in the atmosphere. Unfortunately, the

sensors considered were well outside of our budget limitations and had strict operating temperature windows which would have been difficult to implement. Consequently, we focused on measuring particulate matter as a potential contributor to light attenuation. The Adafruit STEMMA PMSA0031 was selected due to its Qwiic compatibility and a suitable range of particulate sizes measured.

2.2.4 Enclosure

The enclosure was designed in Onshape. The skeleton and templates to cut the foam were 3D printed out of PLA filament. The skeleton included mounts for securely bolting components using M3 fasteners. A bracket was designed to position the light sensor behind the acrylic glass window and an intake/exhaust port was added to give the air particulate sensor access to outside air while keeping the component inside the temperature-controlled area of the enclosure. EVA foam and foam board sections were cut using the printed templates to form a tight fit around the skeleton. Due to PLA's brittleness at low temperatures, the skeleton was used solely for component mounting, with structural integrity provided by the foam exterior. The design was informed by the successful flight of our test kit payload, which used similar materials and construction.

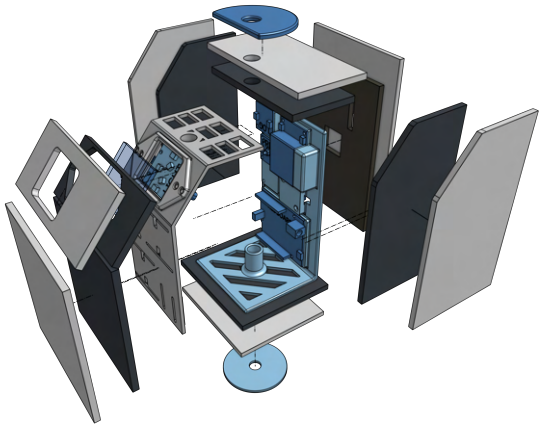

Figure 2.3: Exploded CAD Model

2.3 Software and Electronics Implementation

The code for the sensor array and the heating subsystem were both quite simple which allowed the payload to be easily testable and reliable.

2.3.1 Sensor Array

The sensor array was controlled by a SparkFun RedBoard. Although potentially overkill for this task, it was selected to ensure compatibility with the Qwiic platform we were not yet familiar with. Since we only needed to read data from the sensor and write it to the SD card, and we used the Qwiic standard, once the sensor objects were created we only had to request the data from the sensor and then send it to the SD card. The program checks for the existence of a file named Datalog.txt on the SD card, creates it

if necessary, then prints sensor readings to the file separated by commas. Each set of readings is followed by a newline, enabling easy separation into spreadsheet columns for analysis.

```
void loop() {

  dataLogger.append("DataLog.txt"); // Tells the Arduino that we want to write to DataLog.txt

  digitalWrite(ledPin, HIGH); // Turn on Arduino built-in LED to signify that a data recording loop has started
  delay(1000);

  //**********************************************************************
  // Start of spectral sensor block

  lightSensor.takeMeasurements(); //This is a hard wait while all 18 channels are measured

  //A Band: 410nm
  dataLogger.print("A");
  dataLogger.print(",");
  dataLogger.print(lightSensor.getCalibratedA()); //410nm
  dataLogger.print(",");
```

Figure 2.4: Spectrometer Sample Code

2.3.2 Heating Subsystem

The heating system was controlled by a separate Arduino Pro Micro, as we already had one in possession and had the added benefit of it being lightweight. Its code cycles the nichrome coil on for five seconds whenever the DS18B20 reads a temperature below 5°C, then reassesses the temperature before repeating. The coil was powered by two 9V batteries wired in parallel to deliver 2400 mAh at 9V, sufficient for the flight duration based on our measured current draw. Both microcontrollers shared a third 9V battery (1200 mAh) which was also deemed sufficient after current draw testing.

```
void loop() {

  // Send request for temperature reading to sensor
  tempSensor.requestTemperatures();
  // Store temp in C to internalTemp variable
  float internalTemp;
  internalTemp = tempSensor.getTempCByIndex(0);

  // Print temp to serial
  Serial.println(internalTemp);

  if (internalTemp <= 5) {
    digitalWrite(HEATER_STATUS_LED, HIGH);
    digitalWrite(HEATER_TRIGGER, HIGH);
    digitalWrite(FAN_TRIGGER, HIGH);
    delay(2000);
  }

  // Reset heater status LED and relay trigger pin
  digitalWrite(HEATER_TRIGGER, LOW);
  digitalWrite(HEATER_STATUS_LED, LOW);
  digitalWrite(FAN_TRIGGER, LOW);

  delay(2000);

}
```

Figure 2.5: Heater Sample Code

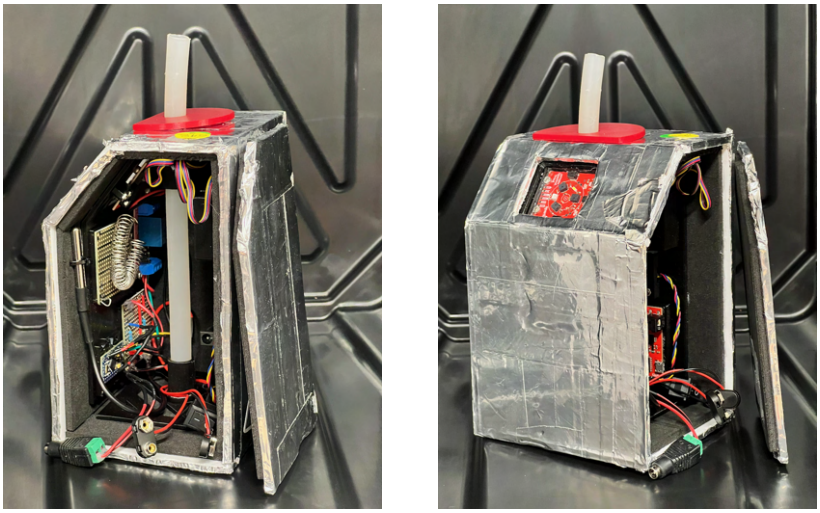

Figure 2.6: Final Payload Build

Section 3

Testing

3.1 Overview

Our tests, in order to determine the survivability and durability of the payload, were focused on three main concerns: cold temperatures, the effects of low air pressure, and how the enclosure design might affect data readings. We implemented vacuum chamber, temperature, and light tests to assess this.

3.2 Vacuum Chamber Test

The vacuum chamber test served to validate the material composition of both the sensors as well as the enclosure. Our enclosure was fabricated using 3D printing. In order to ensure that it would not explode in the low-pressure environment of high altitude, we sealed the device within a vacuum chamber and lowered the pressure to approximately -5 mmHg, a level beyond what we expected our payload to experience. Both the components and the enclosure survived this test with no negative effects. We considered this test a success.

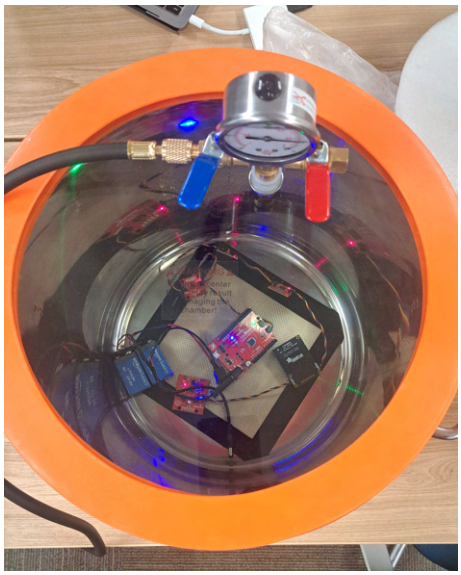

Figure 3.1: Vacuum Chamber Testing: Internal Components

3.3 Temperature Test

3.3.1 Heating Subsystem

For this test, we purchased a Styrofoam cooler and a quantity of dry ice. We placed the heating element inside the cooler and inserted an external temperature probe so that we would be able to monitor the internal temperature while the test was taking place.

The heating device was set to turn on when the internal temperature reached 5° C, and then to remain on for five seconds before taking another temperature reading. If the internal temperature remained at 5° C or below, the heating device would cycle again until the internal temperature read above 5° C. For our temperature test, we wanted to verify that the heating subsystem had been coded properly to turn on at the right temperature and would turn off as instructed.

Figure 3.2: Temperature Testing: Heating Subsystem

We were able to observe the temperature within the cooler fall closer and closer to the 5° C range needed to activate the heating subsystem. As expected, once the temperature dipped below the 5° C threshold, the heating element turned on. It also continued to cycle and check temperatures throughout the 50-minute testing period. Figure 3.3 shows the temperature readings from inside the cooler, along with a horizontal line to indicate the temperature threshold that would have activated the heating element. Due to the heating element operating as expected, we determined this test to be a success.

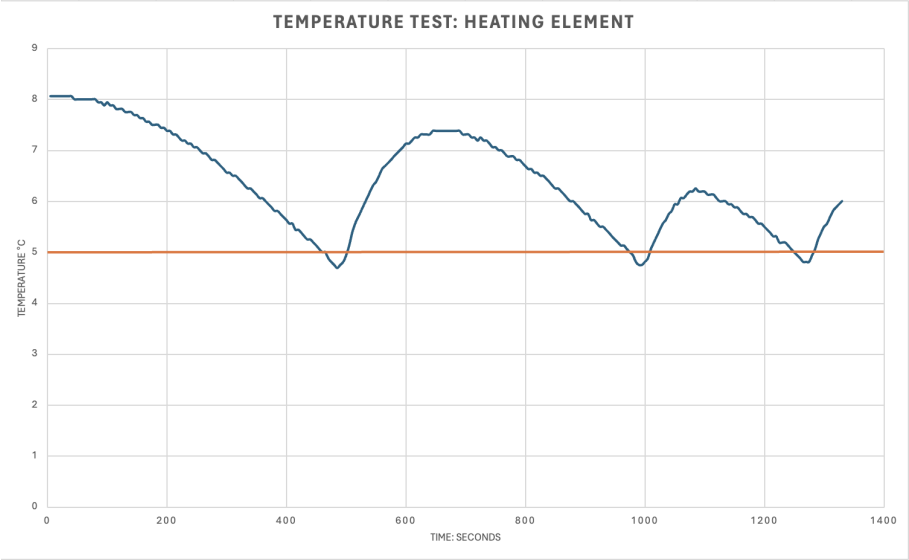

Figure 3.3: Temperature Data Recorded

3.3.2 External Components

The second component of our temperature test involved a materials test for the window built into the design of our enclosure. We wanted to ensure that no condensation would form in the presence of cold temperatures that could influence the ability of our spectrometer to observe and record light data. We also included the portion of the enclosure containing the acrylic window in the cooler as part of our temperature testing. We did not observe condensation on the surface and likewise considered this test to be successful.

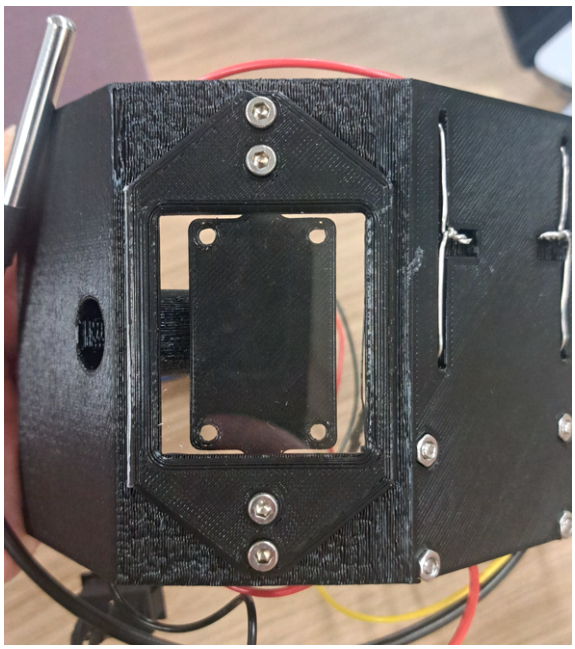

Figure 3.4: Window Clarity Testing

3.4 Light Test

Because our enclosure would require a rigid yet transparent substance to function as a window to let light into the payload, without overly exposing it to atmospheric elements, we completed several tests to ensure that our chosen material, polymethyl methacrylate, would not interfere with our spectrometer's ability to record light data.

We designed three separate tests involving readings of indoor, outdoor, and exclusively infrared light with and without the window.

3.4.1 Indoor Light

The indoor light test revealed the smallest deviation between recorded values, with percent difference between readings ranging between 5 percent to 35 percent and an average difference of 13 percent. The results of the test are shown in Figure 3.5 below:

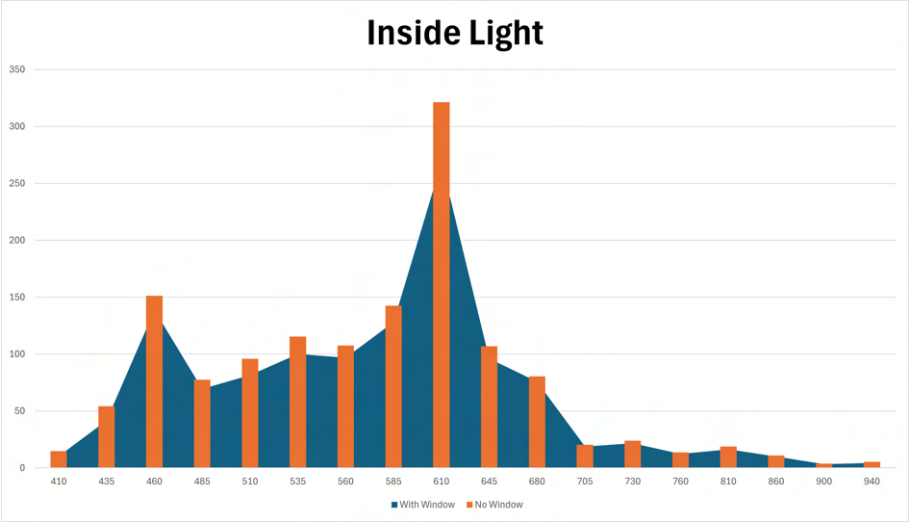

Figure 3.5: Indoor Light Assessment

3.4.2 Outdoor Light

For the outdoor light test, the deviation was much more noticeable, with values ranging from 21 percent to 32 percent with an average difference of 26 percent. In contrast to the indoor light test, the values are much more tightly grouped. The values are shown in Figure 3.6, with the bars indicating light readings without the window, and the gradient representing light readings from behind the window.

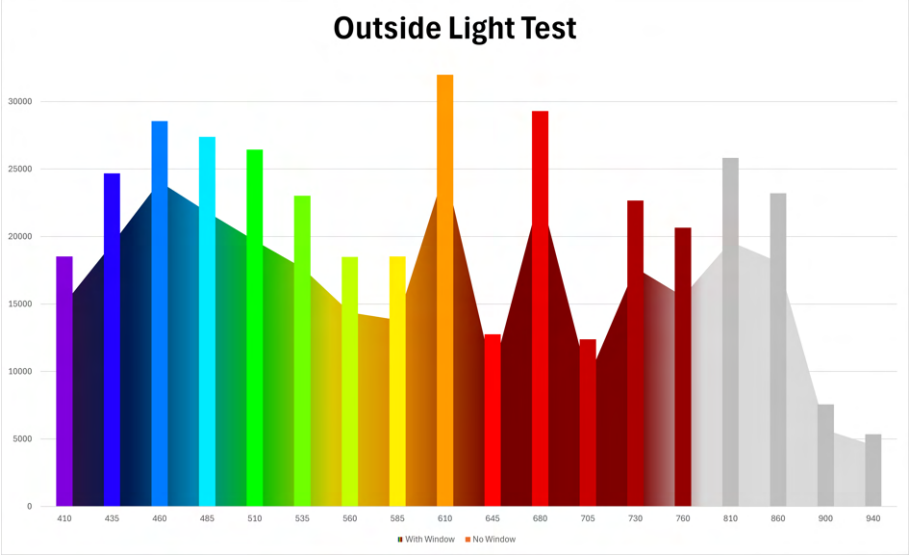

Figure 3.6: Outdoor Light Assessment

3.4.3 Infrared Light

Lastly, the light test readings from the infrared test show the largest deviation, with values averaging 96 percent error. We expect from this test that certain readings may have been severely limited.

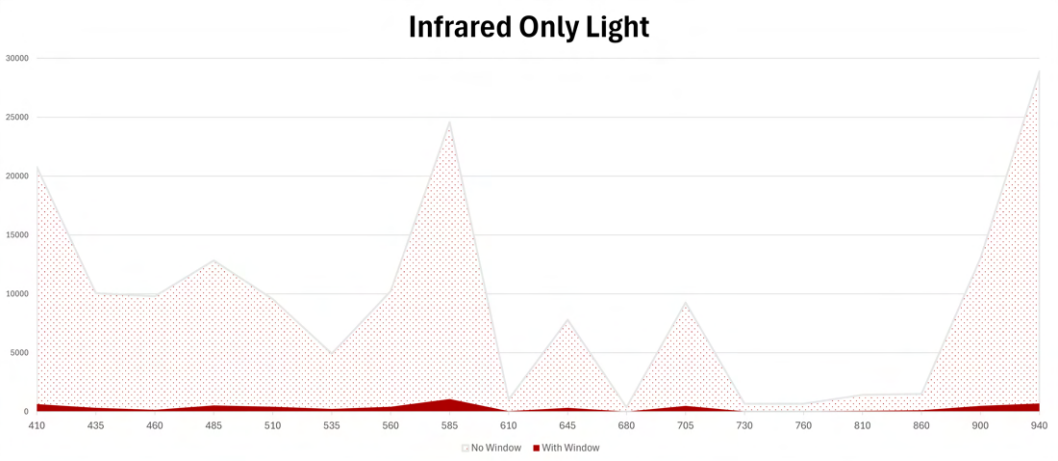

Figure 3.7: Infrared Light Assessment

Despite these deviations, we were confident that we would still be able to obtain meaningful results with the understanding that actual values may be limited by a factor of approximately 26 percent.

Section 4

Results and Analysis

Our payload successfully launched on April 6, 2025 from Deer Trail, Colorado at approximately 7:21am. It achieved a maximum altitude of 94,074 ft and was safely recovered close to Matheson, Colorado. Our results show a variety of information.

4.1 Spectrometer Results

Our spectrometer recorded values by using a relative measure known as “intensity,” described as “counts” per measure of irradiance (recorded in microwatts/cm2). We were able to generate graphs relating intensity to time of flight, which includes initial ascent, peak altitude, and final descent. With a sunrise time of approximately 6:35 am and a launch time of 7:21 am, light intensity continued to increase throughout the day, until landing and retrieval approximately 2.5 hours later.

As such, an initial review of our light data shows intensity readings that increase with time, with a distinct "U" shape in the bottom portion of the graphs, notably most concentrated and lowest in intensity around the time of peak altitude. This may be attributed to refraction effects from denser air regions. With more air molecules present at these lower altitudes, more light was likely refracted into the spectrometer, increasing the intensity, and vice versa with peak altitude. This trend is consistent across nearly all wavelengths and could explain the higher floor of readings at lower altitudes.

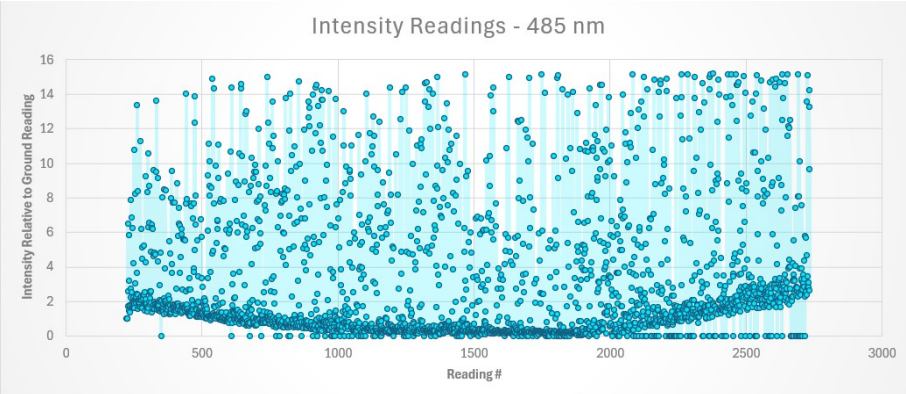

Figure 4.1: Blue Light Intensity

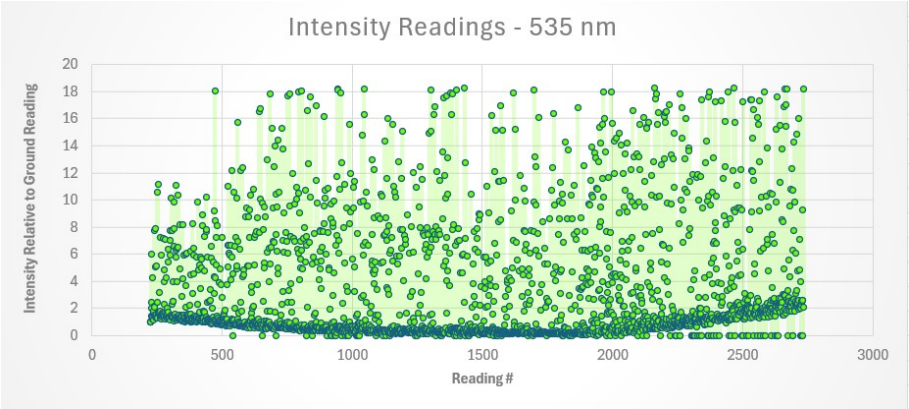

Figure 4.2: Green Light Intensity

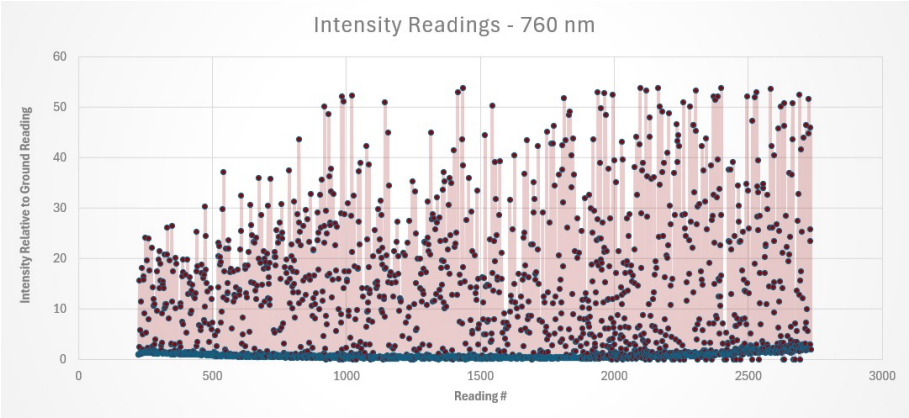

Figure 4.3: Red Light Intensity

Although a pure measure of light intensity did not reveal as direct of a relationship between light and altitude as we would have expected, examining data in the context of irradiance does provide a bit more insight.

One particular measure of light energy exists in the form of irradiance, measured as the amount of energy delivered to one square meter (Serway, 2013). With regard to solar irradiance, a ratio that correlates this energy value per wavelength can also be determined as power per square meter, per wavelength, as shown in Figure 4.4:

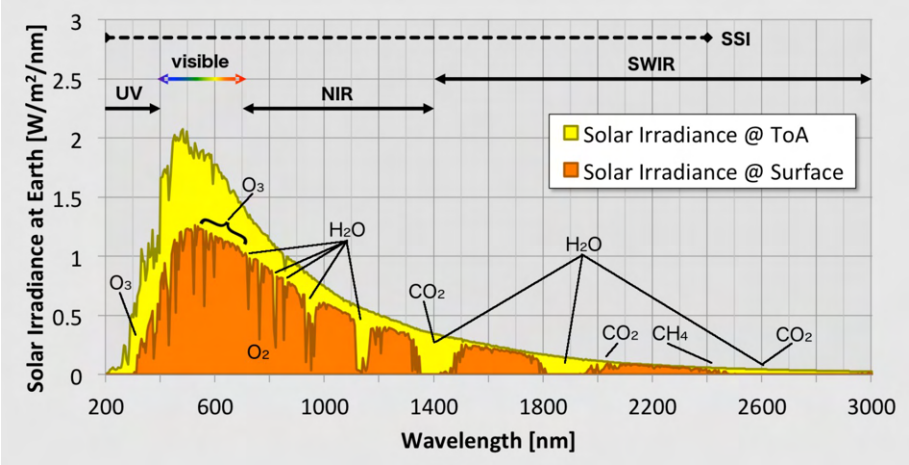

Figure 4.4: Solar Irradiance Trend

Solar Irradiance | Sun Climate. (2018, March 6).
https://sunclimate.gsfc.nasa.gov/article/solar-irradiance

Solar spectral irradiance describes the distribution of the sun's energy across multiple wavelengths within the electromagnetic spectrum ("Solar Irradiance", 2018). Given that our spectrometer recorded values in intensity, described as "counts" per microwatt per centimeter squared, we sought to determine if it would be possible to convert our data into a similar value to the one shown in the Graph above, and then make comparisons concerning our measurements of solar irradiance.

Our spectrometer's datasheet indicated a calibration factor that allowed us to make these unit conversions. Upon dividing these values by wavelength, consistent with Figure 4.4, we were able to generate similar results. The equation used is referenced below:

$$\frac{10 * \left(\frac{\text{Recorded Intensity}}{\text{Calibration Factor}}\right)}{\text{Wavelength}} = \text{Irradiance Value Per Wavelength}$$

$$\text{Calibration Factor} = 35$$

The multiplication by a factor of ten serves to convert microwatts per centimeter squared to the more comparable and standard value of watts per meter squared. The calibration factor of 35 was included in the spectrometer datasheet as the base number of counts returned by each wavelength when calibrated with a light source of known intensity. All intensity values from our data were subsequently converted into irradiance values.

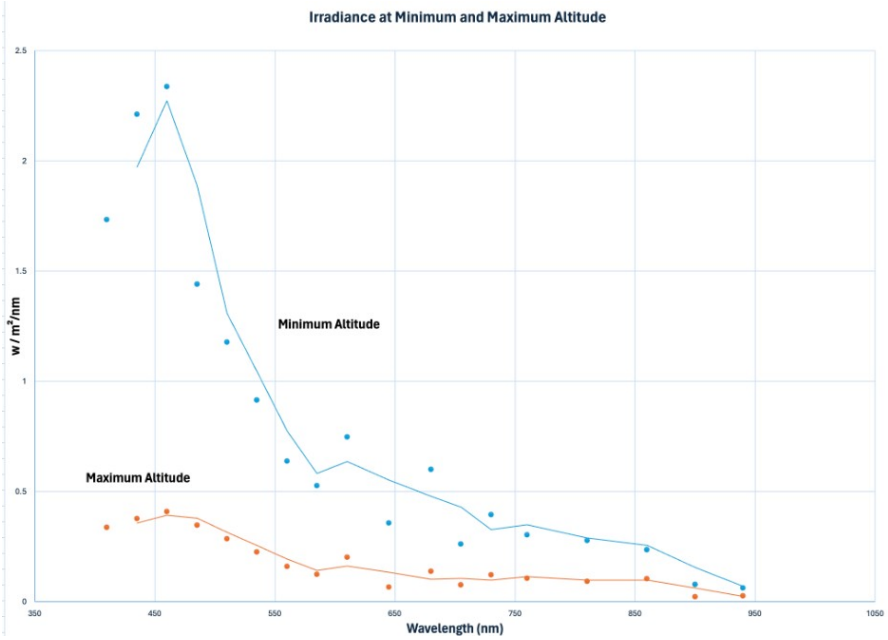

Figure 4.5: Irradiance at Min and Max Alt.

Figure 4.5 indicates irradiance trends taken at two distinct snapshots during the journey of the payload. The blue trend line indicates the irradiance trend near ground level, while the orange trend line reveals trends at near max altitude. A similar survey of data points chosen at random also demonstrate similar behavior at the majority of altitudes sampled.

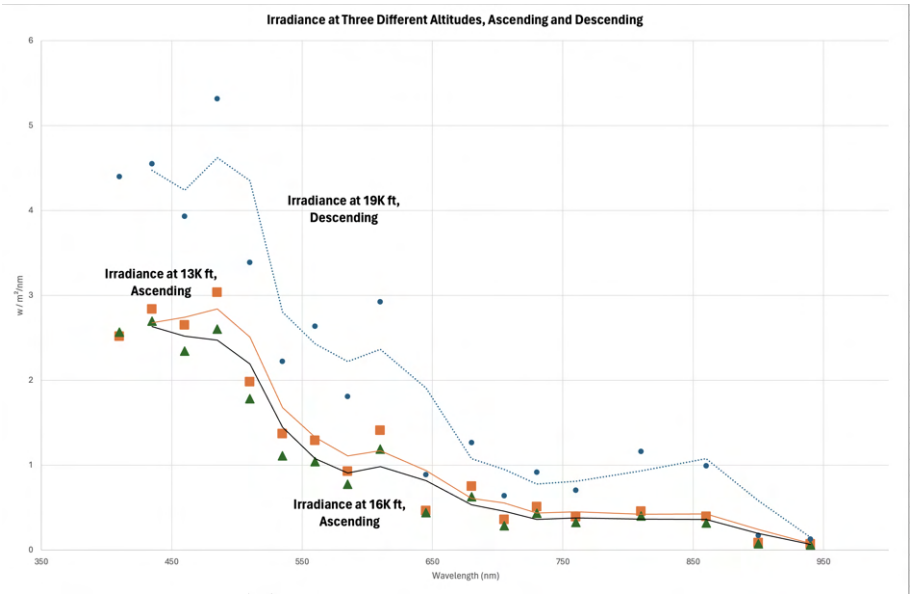

Figure 4.6: Irradiance at Varying Alt.

These trend lines strongly adhere to the shape presented in the NASA irradiance graph shown in Figure 4.4, but with one notable difference. In contrast, our irradiance data decreases with altitude rather than increase. This is one of the more clear determinations of the behavior of light data as it relates to changes in altitude.

However, the data is not free from outliers. Graphs of additional outlier data which reveal high spikes in intensity were both preceded and followed by more homogeneous readings. Interestingly, even within these spikes of unexpected outlier readings, the moving average trend line suggests an overall downward movement, with sinusoidal variation within.

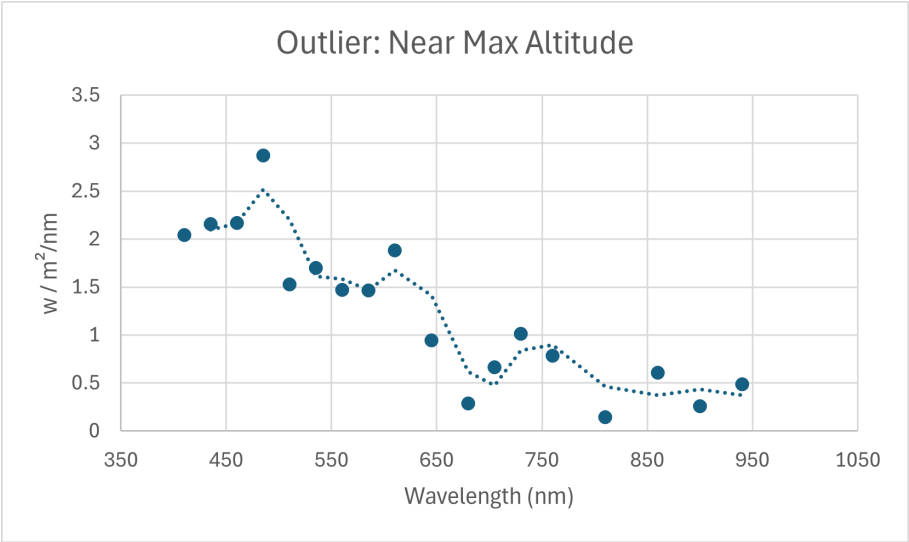

Figure 4.7: Irradiance Outliers

Additional outlier data readings tend to correlate with an absence of data recorded by other sensors, such as the air pressure sensor and the air quality sensor, suggesting that the data recording process as a whole may have been interrupted on a global scale. Many of the data points containing outliers are not included in the analysis for this reason. Regardless, an examination of values in the context of irradiance provides interesting insight into the behavior of light at varying altitudes.

4.2 Particulate Matter Results

The data received was as expected, with similar values compared to the Environmental Protection Agency's data throughout the flight. At ground level the EPA's public data from a nearby testing location showed an average of 51-100 PM2.5 and PM10, while our data showed ranges of 80-200 PM2.5 and PM10 through the first 1,000 feet in altitude gained. This increase may be attributed to a controlled burn directly next to the launch site.

As the payload gained altitude, PM2.5 and PM10 values tapered off steadily, with random spikes showing high values relative to average readings. Near the peak of the payload's ascent, the sensor stopped recording data and did not record any readings for the rest of the flight. We believe this is because the air quality sensor experienced temperatures below its operating temperature of -10℃ to 60℃. Despite our payload having a heated enclosure, the air quality sensor was still taking in outside air which fell as low as -56° C.

Due to inconsistent wind patterns during the morning of the launch, and the lack of comparison data for similar altitudes during descent, we are unable to verify if inconsistencies in the data were influenced by the nearby controlled burn. For PM2.5 and PM10, values

steadily held ranges above 70 with rare dips below 50 until an altitude of 6,000 ft was gained. The highest concentration of particulate matter typically falls in a range of 6,500 ft and lower in elevation (NASA, 2025).

Section 5

Error Evaluation and Discussion

5.1 Error Analysis

We believe that the large variations in light intensity readings received from the spectrometer at higher altitudes could be caused by lower air density and humidity levels leading to reduced light scattering. This would create a case where the light being measured is more directional and the sensor would go between brighter and darker spots as it pointed towards and away from the sun, whereas at lower altitudes light scattering would allow representative readings in pretty much any direction. We presume that the payload was spinning and experiencing turbulence on the flight string, which supports this line of thinking. Spikes in readings could also have been caused by reflections from other payloads, which were also covered in aluminum tape. Due to the configuration of the flight string, it seems unlikely that it would have occurred at the frequency we see in the sensor readings.

During testing, we observed that the acrylic glass window shielding the light sensor had a filtering effect which reduced the amount of light reaching the sensor. The amount of light filtered per wavelength was consistent, which allowed us to adjust the data to compensate for this filtering effect. This is a reason that other window materials were considered, however acrylic glass had the best price to clarity ratio available within our budget.

There was a moderate number of errors in pressure readings during the payload's descent. We observed during vacuum chamber testing that when the pressure sensor was subjected to pressures below its operating window, it experienced more errors after returning to within its operating pressure window. Since the pressures at the top of the ascent were near the bottom end of the sensor's operating window, this may have caused more reading faults during descent.

When comparing our calculated irradiance levels to the graph of NASA's measurements, their data shows high altitude readings to show an overall higher irradiance compared to ground level readings. This is what we expected to see in our data at higher altitudes, however our readings showed a lower intensity at high altitudes compared to ground level. This is likely due to reduced scattering as the payload ascended, as discussed above, combined with our inability to aim the payload towards the sun. NASA's high-altitude sensor is mounted to a two-axis gimbal system on the ISS, which allows a 15-minute measurement window per day where they are able to precisely aim the sensor at the sun. They also measured irradiance directly using three radiometers, rather than reverse-

engineering irradiance values from relative light intensity as was our method. In the design of our experiment, we underestimated the impact that light scattering would have on the level of ambient light available to be measured by a sensor. We did not consider the importance of sensor direction when performing readings in low density atmosphere (Sun Climate, 2017).

5.2 Implications and Applications

Climate Studies: Understanding how light travels through our atmosphere is a key aspect of solar geoengineering, an approach to cooling the earth by reflecting solar radiation back out to space before it can reach the earth. This is one (currently theoretical) response to climate change that would involve intentionally distributing particulate matter into the upper atmosphere to decrease the amount of solar radiation that reaches the earth's surface (UCS, 2020).

Climate models depend heavily on understanding how light filters through the atmosphere to affect our weather patterns. Meteorology uses this information to simulate climate patterns and inform weather predictions. Maintaining an accurate simulation model through regular measurement and observation allows continued accuracy in predictions (USDA).

Aeronautics and Visibility: Information on light intensity per wavelength at various altitudes informs aviation optics research in designing visors and windscreens which strategically filter light and maximize visibility for pilots while reducing exposure to harmful wavelengths (Federal Aviation Administration, 2007). Understanding how light changes with altitude is also crucial for calibrating onboard optical sensors and communication devices which rely on a clear path to the ground (NASA, 1995).

Solar Research: Solar farm placement relies on predicting optimal areas of high irradiance where solar panels are able to efficiently make use of the space. Shorter wavelengths also carry more energy, understanding how different wavelengths are filtered could allow tuning of solar panels to take advantage of wavelengths which are more prevalent in a given area (Ma Lu et al., 2024)

Section 6

Conclusions

This experiment successfully explored the relationship between light intensity and altitude. We measured 18 wavelengths and particulate matter concentrations from the ground to over 90,000 feet. We compared our results to NASA's total solar irradiance data and observed similar spectral trends, with some deviations due to experimental limitations. As expected, light intensity generally increased with altitude, however we underestimated the impact of reduced light scattering on our ability to collect ambient light data. Future missions should take this aspect into consideration to improve the consistency of the data. Despite these constraints, the results provide useful insights into how atmospheric composition affects light transmission with altitude. Measurements like these provide the foundation for research in atmospheric modeling, climate monitoring, and high-altitude optics with applications in aeronautics, climate science, space flight, and solar energy.

Section 7

References

- Air pollution. (n.d.). Retrieved April 13, 2025, from https://www.who.int/health-topics/air-pollution
- Air Quality Index (AQI) | AirNow.gov. (n.d.). Retrieved April 14, 2025, from https://www.airnow.gov/aqi/
- Basics of Global Climate Models | USDA Climate Hubs. (n.d.). Retrieved April 14, 2025, from https://www.climatehubs.usda.gov/hubs/northwest/topic/basics-global-climate-models
- Climate Science Investigations South Florida—Energy: The Driver of Climate. (n.d.). Retrieved April 13, 2025, from https://www.ces.fau.edu/nasa/module-2/radiation-sun.php
- Earth Science Data Systems. (2024a, September 30). Air Quality | NASA Earthdata [Topic Page]. Earth Science Data Systems, NASA. https://www.earthdata.nasa.gov/topics/atmosphere/air-quality
- Earth Science Data Systems. (2024b, October 2). Air Quality Near Real-Time Data | NASA Earthdata [Basic page]. Earth Science Data Systems, NASA. https://www.earthdata.nasa.gov/topics /atmosphere/air-quality/near-real-time-data
- Haering, E. A. (1995, December). Airdata Measurement and Calibration. [Technical Memorandum]. NASA. Retrieved April 14, 2025 from https://ntrs.nasa.gov/api/citations/19990063780/downloads/19990063780.pdf
- Ma Lu, S., Amaducci, S., Gorjian, S., Haworth, M., Hägglund, C., Ma, T., Zainali, S., & Campana, P. E. (2024). Wavelength-selective solar photovoltaic systems to enhance spectral sharing of sunlight in agrivoltaics. Joule, 8(9), 2483–2522. https://doi.org/10.1016/j.joule.2024.08.006
- Mlawer, E. J., Mascio, J., Turner, D. D., Payne, V. H., Flynn, C. J., & Pincus, R. (2024). A More Transparent Infrared Window. Journal of Geophysical Research: Atmospheres, 129(22), e2024JD041366. https://doi.org/10.1029/2024JD041366
- Nakagawara, V. B., Montgomery, R. W., & Marshall, W. J. (2007, July). Optical Radiation Transmittance of Aircraft Windscreens and Pilot Vision. Federal Aviation Administration. Retrieved April 14, 2025 from https://apps.dtic.mil/sti/tr/pdf/ADA471609.pdf

- Rayleigh Scattering. (n.d.). Retrieved April 14, 2025, from https://acd-ext.gsfc.nasa.gov/anonftp/acd/daacozone/Lecture4/Text/Lecture4/rayleigh.html
- Roostaei, V., Gharibzadeh, F., Shamsipour, M., Faridi, S., & Hassanvand, M. S. (2024). Vertical distribution of ambient air pollutants (PM2.5, PM10, NOX, and NO2); A systematic review. Heliyon, 10(21), e39726. https://doi.org/10.1016/j.heliyon.2024.e39726
- Schmucki, D. A., & Philipona, R. (2002). Ultraviolet radiation in the Alps: The altitude effect. Optical Engineering, 41(12), 3090–3095. https://doi.org/10.1117/1.1516820
- Serway, R.A., & Jewett, J.W. (2013). Principles of Physics: A Calculus-Based Text (5th Ed.). Cengage.
- Solar Irradiance | Sun Climate. (2018, March 6). Retrieved April 13, 2025, from https://sunclimate.gsfc.nasa.gov/article/solar-irradiance
- SparkFun (2018, July 9). AS7265x Smart 18-Channel VIS to NIR Spectral ID 3-Sensor Chipset with Electronic Shutter. [Datasheet]. SparkFun Electronics. https://cdn.sparkfun.com/assets/c/2/9/0/a/AS7265xDatasheet.pdf
- Turgut, Enis & Usanmaz, Öznur. (2016). An Analysis of Altitude Wind and Humidity based on Long-term Radiosonde Data. ANADOLU UNIVERSITY JOURNAL OF SCIENCE AND TECHNOLOGY A - Applied Sciences and Engineering. 17. 830-830. 10.18038/aubtda.279852.
- United States Environmental Protection Agency. (2016, March 7). Particulate Matter (PM) Pollution [Collections and Lists]. EPA. https://www.epa.gov/pm-pollution
- United States Environmental Protection Agency. (2017, January 25). Air Quality [Collections and Lists]. EPA. https://www.epa.gov/air-quality
- What is Solar Geoengineering? (2020, October 9). Union of Concerned Scientists. Retrieved April 14, 2025, from https://www.ucs.org/resources/what-solar-geoengineering
- Wild, M. (2009). Global dimming and brightening: A review. Journal of Geophysical Research: Atmospheres, 114(D10). https://doi.org/10.1029/2008JD011470